ResearchGate

See discussions, stats, and author profiles for this publication at: https://www.researchgate.net/publication/329819113

Temperature triggered stoichiometry-dependent desorption from the growth interface of nanofilm

Article *in* Journal of Applied Physics · December 2018

DOI: 10.1063/1.5054998

CITATIONS
0

READS
41

6 authors, including:

Chong Liu
Chinese Academy of Sciences

18 PUBLICATIONS **252** CITATIONS

SEE PROFILE

All content following this page was uploaded by Chong Liu on 23 December 2018.

The user has requested enhancement of the downloaded file.

Temperature triggered stoichiometry-dependent desorption from the growth interface of nanofilm

Chong Liu,[1,2,a)] Lianhong Wang,[1,2] Yitao Zheng,[1,2] Dandan Zeng,[1,2,3] Jianzheng Jiang,[1,2] and Jing Fan[1,2,a)]
[1]*State Key Laboratory of High Temperature Gas Dynamics, Institute of Mechanics, Chinese Academy of Sciences, Beijing 100190, China*
[2]*School of Engineering Science, University of Chinese Academy of Sciences, Beijing 100049, China*
[3]*Academy of Opto-Electronics, Chinese Academy of Sciences, Beijing 100094, China*

(Received 5 September 2018; accepted 5 December 2018; published online 20 December 2018)

In this study, the desorption behaviors of codeposited atoms from the growth interface of multicomponent-nanofilms have been explored through the experiments of vapor codeposition and molecular dynamics simulations. Experimentally, the stoichiometry-dependent desorption has been observed for atoms with weak surface binding, and it appears to be triggered by higher growth temperature, as inferred from the dependence of the amount of deposition on the stoichiometry of precursor films under different conditions. Numerically, we demonstrate that the sticking coefficient of weakly binding atoms depends strongly on the stoichiometry under high growth temperature. However, as the temperature decreases, the sticking coefficient becomes less sensitive to stoichiometry. The mechanisms associated with all the above phenomena have also been discussed. *Published by AIP Publishing.* https://doi.org/10.1063/1.5054998

I. INTRODUCTION

Nanofilms are thin material layers with thickness ranging from a single atomic layer to several hundred nanometers. As the merits of nanofilms arise from different nanostructures, growth control of these nanostructures is known to be of fundamental interest to tune film properties and functionalities. Efforts have therefore been directed toward the synthesis of new functional nanofilms for both scientific research and industrial applications.[1,2] Unlike the widely used structural materials, nanofilms are usually used as functional materials, and owing to this, the focus of nanofilm research has shifted from their mechanical properties[3–6] to intriguing physical properties and related applications, such as novel photocurrent generation material,[7,8] high temperature superconductivity,[9] and ferromagnetic films promising for data storage devices.[10] Most of the functional nanofilms consist of multi-components, in which different atoms and ions are bonded to each other, forming microscale atomic structures.[11–13] The functional properties of nanofilms, including their magnetic properties,[14–16] superconductivity,[17,18] thermal conductivity,[19] and optical properties,[20] arise from their atomic structure and bonding characteristics, which in turn could be tuned by varying their compositions.[16,18,19,21] Therefore, the composition of nanofilms is of vital importance to their functional properties and applications, and hence it is crucial to control the composition during the synthesis of nanofilms.

So far, vapor codeposition has become one of the most versatile approaches to synthesize functional nanofilms with multiple components.[1,22] In a typical codeposition process, several possible phenomena were shown to hinder the control of stoichiometry during the synthesis: (i) changes in the state of the evaporation source may alter the rate of evaporation; (ii) the occurrence of strong scattering upon collision with gaseous molecules inside the vacuum chamber;[23] and (iii) the desorption of adatoms as well as the desorption of admolecules from the growth interface. Admolecule desorption, in turn, can be the result of adatom/adatom association and desorption,[24] adatom/surface-atom desorption (e.g., N_2 desorption from transition metal nitride surfaces in the nitrogen atmosphere and CO desorption from transition metal carbide surfaces exposed to oxygen), which causes the removal of anion surface atoms and formation of anion surface vacancies,[25–29] or gas atom impinging on, bonding to, and removing an adatom.[30,31] The first two mechanisms can be ruled out, as the ejected flux from the evaporation source is tuned by a quartz crystal oscillator, and strong collision scattering can be suppressed by reducing the pressure in the chamber. However, the third origin, i.e., the desorption from the growth interface, cannot be easily monitored or controlled *in situ* and strongly affects film compositions.

The desorption phenomena are still under intensive study from both the experimental and theoretical points of view.[32,33] It is well known that a lower substrate temperature favors adsorption on the growth interface. As a result, the effects of desorption in controlling the composition seem to be trivial in this case. However, to synthesize some of the functional crystals, the deposited atoms were shown to undergo reconstruction of nanostructures,[11] which requires the temperature of the substrate to be increased sufficiently high in order to enhance atomic diffusion.[34] In addition, a higher growth temperature can also assist the deposited atoms to overcome the large potential barrier for different reactions, which consequently facilitates the formation of expected functional crystals. With these physical considerations, a high

[a)]Authors to whom correspondence should be addressed: chongliu@imech.ac.cn and jfan@imech.ac.cn

growth temperature is indispensable for synthesizing some nanofilms.[34,35] However, when the substrate is maintained at a high temperature, the competition between the kinetic energy of adatoms and the surface binding energy complicates the dynamics of adsorbates near the growth interface,[36–38] which may cause atomic desorption and difficulty to control the composition.[39,40] Therefore, it is important to reveal the role of stoichiometry on the desorption behaviors at high temperatures, which will be the focus of our present work.

In this study, both numerical simulations and experiments were conducted to investigate the desorption behaviors of atoms from the growth interface. The vapor codepositions of Cu, Y, and BaF_2 on $LaAlO_3$ were studied experimentally under a wide range of temperature from 25 to 600 °C. It has been found that the amount of deposition of Cu is sensitive not only to the growth temperature but also to the stoichiometry of the precursor films. However, this stoichiometry-dependent desorption phenomenon disappears when the growth temperature is low. To understand this temperature-triggered stoichiometry-dependent desorption, we simulated vapor codeposition of binary species of atoms, using molecular dynamics (MD) simulations, with different binding strengths. A distinct dependence of sticking coefficient on the ratio of incident flux of A atoms to that of B atoms (γ_A/γ_B) has been found out. However, as the growth temperature decreases, the sticking coefficient becomes less sensitive to the ratio of γ_A/γ_B. In addition, our numerical results also show that the adsorption behaviors are highly nonlinear with time due to the evolution of the growth interface.

II. EXPERIMENT

Our codeposition system utilized in this study is shown schematically in Fig. 1, which consists of a vacuum chamber, monitors, and controlling devices. The vacuum chamber is divided equally into three regions, in each of which the evaporant is placed in a crucible, as illustrated in Fig. 1(a). The evaporation of Y and Cu was achieved by electron guns, whereas a thermal resistance heater was utilized to evaporate BaF_2 to prevent the breakage of ionic bonds. To circumvent strong scattering and to ensure a higher performance of the electron gun, the pressure in the chamber was maintained at or below 3×10^{-3} Pa. Quartz crystal oscillators in each of the regions were employed as sensors to detect incident flux. By comparing the detected flux with the desired values, the controller could adjust the power of electron-guns and thermal resistance heaters.[41] Through this approach, the incident flux evaporated from each individual source could be effectively controlled.

The precursor films were deposited on (100) $LaAlO_3$ (LAO) substrates, which could facilitate the epitaxial growth of $YBa_2Cu_3O_7$ (YBCO) in the subsequent annealing progress, due to similar lattice parameters between LAO and YBCO. The LAO substrates were fixed on a substrate disk in the top region of the vacuum chamber, as illustrated in Fig. 1(b). Using a thermal resistance heater, which was installed adjacent to the substrate disk, the substrate was heated uniformly to a desired temperature, and the

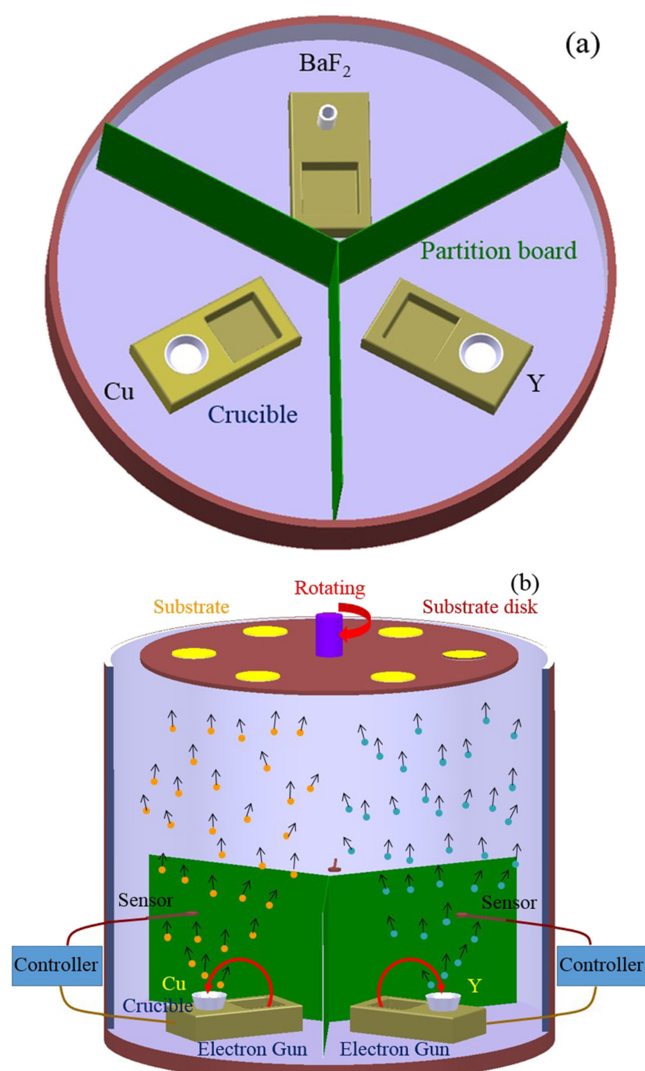

FIG. 1. The schematic for vapor codeposition of multicomponent nanofilms. The vacuum chamber is divided equally into three evaporation regions by the partition board. Y and Cu are placed in molybdenum crucibles, and BaF_2 is in a boron nitride crucible. (a) Top view and (b) front view.

temperature was monitored by a pyrometer. As the substrate disk rotates around its axis at a constant speed of 90 revolutions per minute, the substrate passed through different evaporation regions and was exposed to the incident flux of each individual source successively with equal time. With this approach, the elements from different evaporation sources can be uniformly mixed on the substrates. After each codeposition, the number of atoms of each element deposited on the substrate could be obtained by inductively coupled plasma atomic emission spectroscopy (ICP-AES) analysis.

The codeposition of Y, BaF_2, and Cu was performed under different growth temperatures from 25 to 600 °C. To understand the effects of the growth temperature, other conditions for the deposition were kept constant, including the incident flux and the rotational speed of the substrate disk. The number of atoms of each element deposited on the substrate is scaled by the substrate area, and the thickness was recorded by a film thickness controller. The reduced number of atoms (φ) is plotted as a function of substrate temperature (Fig. 2). It is seen that as the substrate temperature increases,

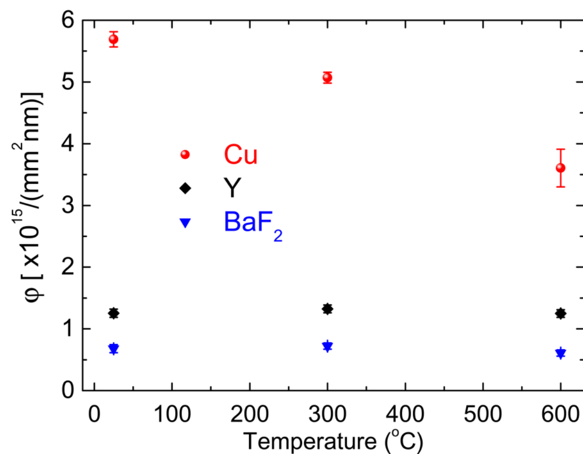

FIG. 2. The reduced number of atoms adsorbed on the substrate versus temperature. The number of atoms of each element is scaled by the substrate area and thickness recorded by a film thickness controller. The error bars are estimated by the standard deviations of ICP-AES results.

the amount of Cu deposition decreases. Nevertheless, for BaF_2 and Y, φ does not change significantly with the substrate temperature. This indicates that the role of temperature on the amount of deposition is only sensitive for some of the elements, which requires further detailed investigations.

III. MOLECULAR DYNAMICS SIMULATIONS

To understand the above observation, molecular dynamics (MD) simulations were employed to study atomic dynamics at the growth interface during vapor codeposition, using the Large scale Atomic/Molecular Massively Parallel Simulator (LAMMPS).[42] The MD model consists of the substrate and deposited atoms,[43–46] as illustrated in Fig. 3. To consider a more general case, the material system used in MD simulation is different from that in the experiment. Five layers of body centered cubic (bcc) Fe atoms with a lattice parameter of 2.867 Å are used to model the substrate surface, shown as the red particles in Fig. 3(b). The embedded-atom method (EAM) force field is employed to calculate the thermal vibration of the substrate atoms,[47] which affects the energy accommodation of the substrate atoms and dynamics of the adatoms. The deposited atoms are modeled by the Lennard-Jones (LJ) potential, $U(r) = 4\varepsilon[(\sigma/r)^{12} - (\sigma/r)^6]$, where r is the separation between a pair of molecules, σ is the collision diameter, and ε is the binding energy. The interaction between the deposited and the substrate atoms is also calculated by the LJ potential, and the Lorentz-Berthelot mixing rule is used to calculate the interaction parameters.[48,49] In order to implement the mixing rule for the gas-substrate interactions, LJ parameters in Ref. 50 are used for both the evaporated and substrate atoms. To explore the surface effects caused by different substrate materials, an approach similar to Ref. 48 is employed to model different strengths of surface effect through varying gas-substrate binding energies. It is also noted that, as the evaporated gas atoms collide with the surface, some of them may be adsorbed on the substrate and become solid atoms. In this case, the adatom-adatom interactions on solid surfaces often

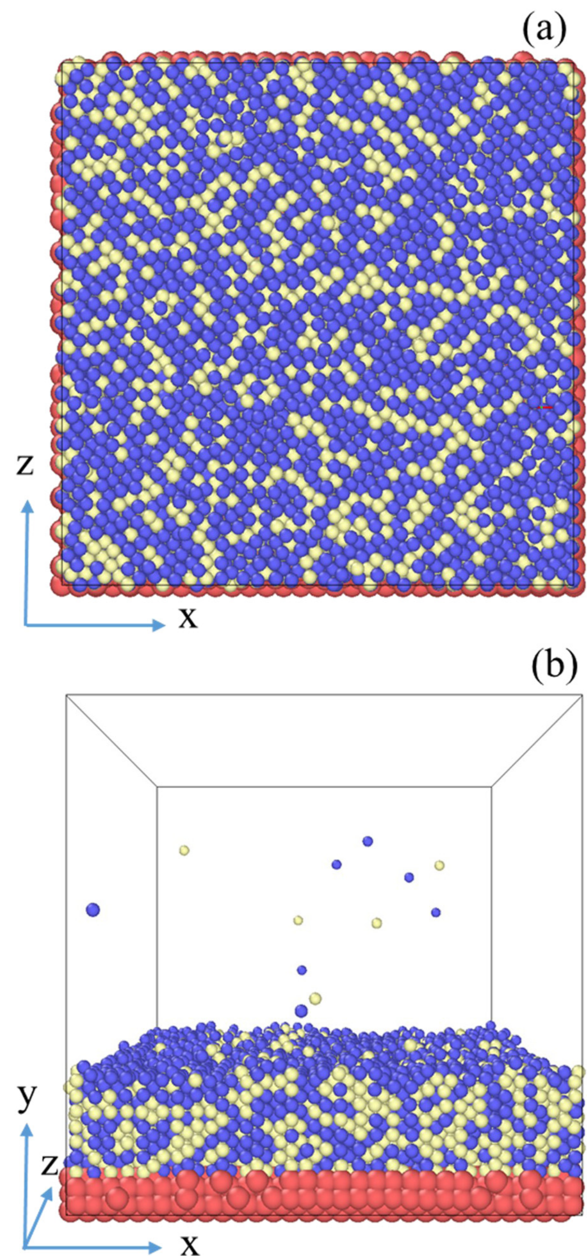

FIG. 3. Molecular dynamics simulation model of a typical vapor codeposition system. Red particles are substrate atoms; yellow and blue particles denote different species of evaporant atoms.

exhibit a non-trivial long-range oscillatory behavior,[51] which cannot be captured by the LJ potential, and hence more fundamental methods, e.g., *ab initio* molecular dynamics simulations, are required to investigate the transport and nucleation of adatoms. However, in our work, the adsorption of gas molecules mainly depends on gas-substrate interactions, and *therefore* the transport and nucleation of adatoms, which is governed by adatom-adatom interactions, are of secondary importance to the adsorption of gas atoms.

The planar substrate is placed at the bottom of the simulation box [Fig. 3(b)]. The atoms in the bottom-most layer are fixed to maintain a stable system, whereas atoms in the other four layers are free to vibrate to consider the energy accommodation of the substrate. The initial velocities of the substrate atoms follow Maxwell-Boltzmann distribution

corresponding to the substrate temperature. The temperature of the substrate is maintained at a desired value by applying a Nose-Hoover thermostat to the vibrating substrate atoms only. The atoms to be deposited are inserted randomly at the top region with initial velocities between 500 m/s and 600 m/s along the negative y direction. Newton's equations are integrated with a time step of 1 fs. The size of the substrate is about 8.6 nm × 8.6 nm, and the length of the simulation system in the y direction is about 8.6 nm. Periodic boundary conditions are applied in the x and z directions.

Single element deposition was first simulated to explore the influence of growth temperature on the desorption of atoms under different surface conditions. The sticking coefficient is estimated by the ratio of the number of adsorbate atoms to the total number of incident atoms during the simulation period. Figure 4 shows the sticking coefficient as a function of substrate temperature with three different binding energies. It is seen that all the curves of the sticking coefficient can be divided into three regions, i.e., complete adsorption region, no adsorption region, and the transition region where the sticking coefficient is reduced from one to almost zero as the temperature increases. When the binding energy is small, this transition takes place in the low temperature region. However, for the case of strong binding, the transition region shifts toward higher temperatures, which may be beyond the range of commonly used temperatures for film growth, as shown by the black curve in Fig. 4.

Based on the above analysis, the observed phenomena in our studies can be explained as follows. Compared with Cu, Y and Ba are much easier to be oxidized,[52,53] which indicates that Y and Ba are more prone to combine with negative ions (e.g., oxygen ions, O^{-2}, or fluoride ions, F^{-1}) through forming chemical bonds. Therefore, chemical adsorption is more favorable for Y and Ba. Typically, the binding strength of chemical adsorption is much stronger than that of physical adsorption where van der Waals force dominates.[39] For the case of strong binding, the transition from complete adsorption to no adsorption takes place in the region of high temperature, as shown by the black curve in Fig. 4. Thus, within the range of deposition temperature (25 to 600 °C), the sticking coefficient does not change significantly (Points A to B in Fig. 4). This explains why the amounts of deposition of Y and BaF_2 are insensitive to temperature. On the other hand, when the surface binding is weak, the transition occurs at a relatively low temperature, which is within the range of deposition temperature. From Points A to C in Fig. 4, as the temperature increases, a decrease in the sticking coefficient is evident. Consequently, the amount of Cu deposition decreases as the temperature increases. This also justifies our previous preliminary interpretation that the difficulties in controlling the composition for high-temperature growth are caused by atomic desorption, which can be greatly affected by both the growth temperature and binding strength.

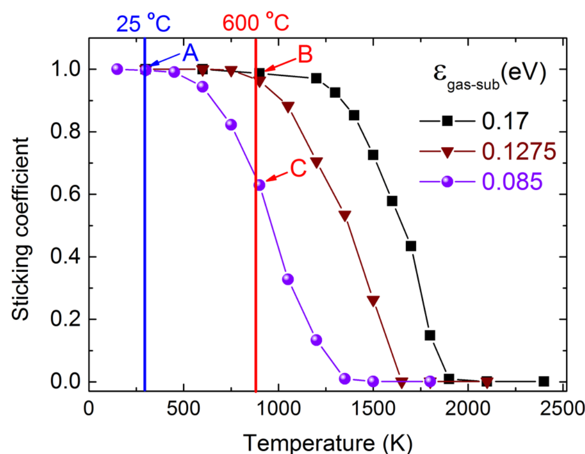

FIG. 4. The sticking coefficient as a function of growth temperature under different strengths of gas-substrate binding. The results are obtained by molecular dynamics simulation of vapor deposition.

IV. STOICHIOMETRY-DEPENDENT DESORPTION

As high temperature makes the dynamics of atoms at the growth interface complicated, an intriguing stoichiometry-dependent phenomenon is also observed in our codeposition experiments. To consider the effects of stoichiometry, the incident flux of Cu is fixed while varying the incident flux of BaF_2 in each of the codeposition experiments. It is seen that the amount of deposition of Cu decreases almost linearly with increasing mole fraction of BaF_2 [Fig. 5(a)],

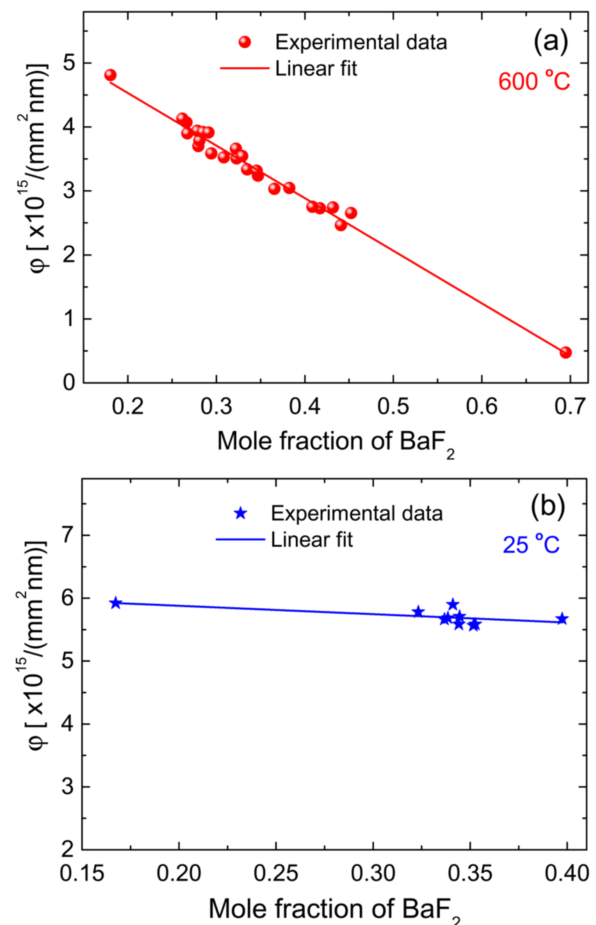

FIG. 5. The reduced number of atoms of deposited Cu versus the mole fraction of BaF_2. The amount of deposition of Cu is scaled by the substrate area and thickness was recorded by a film thickness controller. (a) and (b) are experimental results conducted under 600 °C and 25 °C, respectively, whose linear fit to the experimental data is also shown.

which reveals that the dynamics of Cu atoms on the growth interface can be greatly altered by the stoichiometry of precursor films. This intriguing observation requires a detailed analysis on the influence of variations in surface binding. In the initial deposition stage, the substrate surface is almost clear, and the interaction between the evaporated and the substrate atoms is dominant. With a progress in the deposition, the substrate is covered by a thickening layer of adsorbates, which separates the direct interaction between the evaporated and substrate atoms.[54] Therefore, in the stage of complete coverage, the dominant surface binding becomes gas-adsorbate binding, which depends on the interactions between the evaporated atoms and adatoms on the growth interface.[33] In this case, the strength of gas-adsorbate binding is not only dependent on the type of atoms to be deposited[55] but also influenced by the stoichiometry of the adsorbates.[56]

The variations in the stoichiometry of adsorbate may also alter its atomic structure and bonding characteristics, and consequently the strength of surface binding. From the observed trend in Fig. 5(a), it could be speculated that an increase in the atomic fraction of BaF_2 may weaken the binding between the adsorbates and evaporated atoms. At a high growth temperature (e.g., 600 °C), a decrease in the surface binding could reduce the sticking coefficient, as evidenced by the change from point B (black curve) to point C (purple curve) shown in Fig. 4. Therefore, the amount of deposition of Cu decreases with an increase in the mole fraction of BaF_2.

However, when the above experiment was conducted under room temperature, the amount of Cu deposition becomes less sensitive to stoichiometry, as shown in Fig. 5(b). To understand this, changes in the sticking coefficient at low temperature range were checked, and it is shown that all the curves of the sticking coefficient for different binding energies converge to unity, irrespective of how the binding energy is altered with changes in the adsorbates (Fig. 4). Consequently, the sticking coefficient does not change considerably with varying binding energies (the intersection of the blue line with other curves in Fig. 4). This is a possible interpretation for why the amount of deposition of Cu becomes less sensitive to the mole fraction of BaF_2 at room temperature.

To further understand this observation, molecular dynamics simulations were utilized to investigate the binary codeposition processes with different ratios of incident flux. Two types of evaporated atoms with different binding strength are considered in the simulation, and the potential parameters of Ni[50] are employed to model the strong binding atoms, denoted as A species ($\varepsilon = 0.529$ eV, $\sigma = 2.22$ Å). Since the self-binding energy for most of the popular metals is greater than or of the order of the growth temperature (kT), the binding energy (ε) for Cu[50] is scaled by a factor to model the weak binding case, denoted as B species ($\varepsilon = 0.0415$ eV, $\sigma = 2.277$ Å). The effects of stoichiometry on desorption are considered through changing the ratio of incident flux of A and that of B (γ_A/γ_B). The results are shown in Fig. 6. The sticking coefficient of A and B under different γ_A/γ_B is plotted as a function of temperature. When $\gamma_A/\gamma_B = 1$ and $T = 300$ K, the sticking coefficients for both A and B are close to 1, which indicates the occurrence of no evident desorption. As the temperature increases, the sticking coefficient of B decreases much faster than that of A, revealing that the sticking coefficient is more sensitive to temperature for weakly binding atoms. As γ_A/γ_B is increased or reduced from 1, the sticking coefficient for both A and B moves up or down correspondingly (Fig. 6). This confirms that the desorption behaviors are stoichiometry dependent, which is further evidenced by the dependence of the sticking coefficient on γ_A/γ_B as depicted in Fig. 7. These numerical results confirm our previous explanations for the stoichiometry dependent desorption.

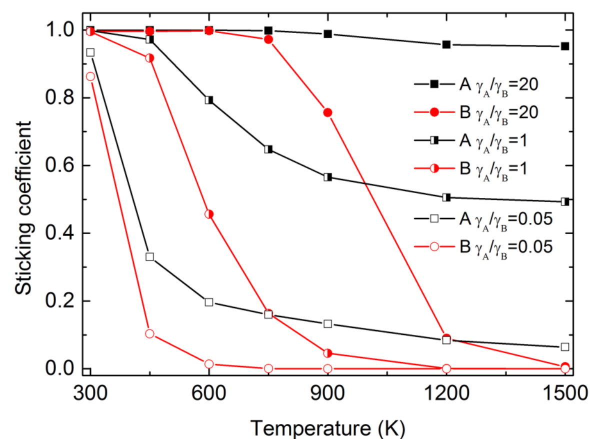

FIG. 6. The sticking coefficient of adsorbates A and B as a function of temperature under different ratios of incident flux γ_A/γ_B. The symbols are the MD simulation results at 600 K, and the solid curve is a guide to the eye.

It is also noted that the sticking coefficient is estimated on a time-average basis. In fact, the sticking coefficient may not be constant during codeposition, due to the evolution of the growth interface. To illustrate this nonlinear phenomenon, the number of atoms adsorbed on the substrate N under different γ_A/γ_B was examined. Figure 8 shows the reduced number of adsorbed atoms N/N_0 as a function of time, where N_0 is the total number of atoms impinging on the growth interface. It is seen that there is a critical time (about 0.6–0.7 ns) which divides the deposition process into

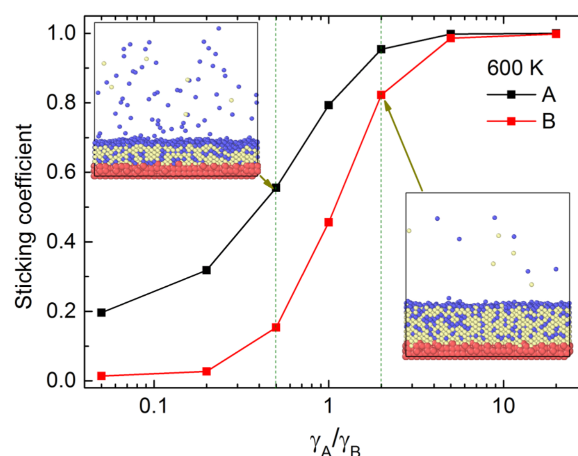

FIG. 7. The sticking coefficient of adsorbates A and B as a function of γ_A/γ_B. The insets illustrate the atomic structures after each codeposition under different γ_A/γ_B, for the upper left snapshot $\gamma_A/\gamma_B = 0.5$ and for the lower right snapshot $\gamma_A/\gamma_B = 2$; the yellow particles represent A atoms, and the blue particles represent B atoms.

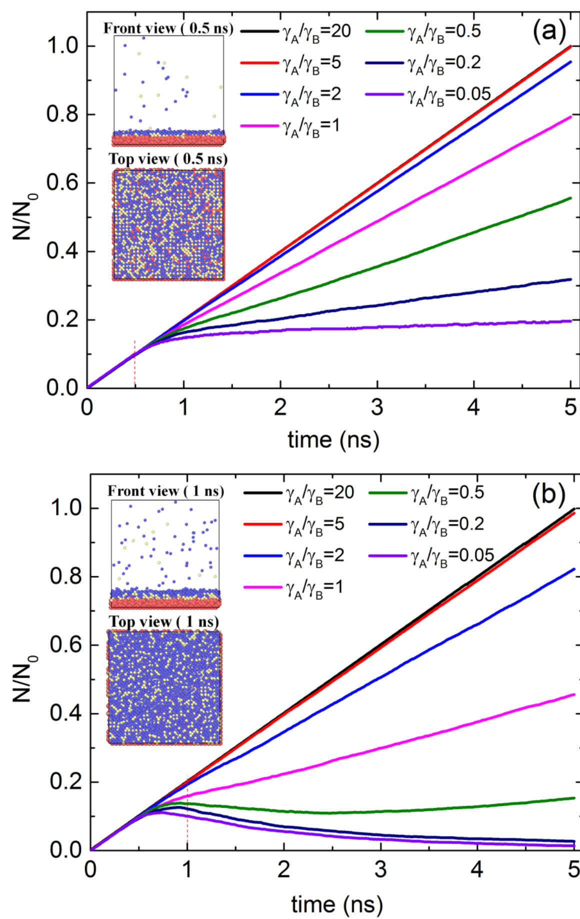

FIG. 8. Reduced number of adsorbed atoms (N/N_0) of A atoms (a) and B atoms (b) as a function of deposition time under different γ_A/γ_B, where N is the number of atoms adsorbed on the substrate and N_0 is the total number of atoms impinging on the growth interface. The snapshots in (a) and (b) are the molecular structure of films at 0.5 ns and 1 ns, respectively, and the yellow and blue particles represent A and B atoms, respectively.

two regions, where the influence of γ_A/γ_B on desorption is different. Before the critical time is the early stage where the coverage is low [the inset in Fig. 8(a)], the reduced number of adsorbed atoms N/N_0 for both A and B is independent of γ_A/γ_B and increases almost linearly with time. However, after the critical time, the substrate surface reaches complete coverage, as illustrated by the inset in Fig. 8(b). The reduced number of adsorbed atoms N/N_0 for both A and B diverges to different curves for different γ_A/γ_B and varies nonlinearly with time, especially when γ_A/γ_B is small. This nonlinear phenomenon can be attributed to the variation in the surface binding induced by the evolution of the growth interface, which can be altered by γ_A/γ_B. In addition, it is expected that this nonlinear phenomenon becomes unimportant when the film thickness is sufficiently large and the impact of early-stage non-equilibrium is negligible. The critical film thickness, below which the effect of early-stage non-equilibrium cannot be neglected, is beyond the scope of this current work and will be explored in the future.

V. SUMMARY

In summary, our investigations on the combined vapor codeposition experiments and MD analysis of multicomponent nanofilm growth provide detailed insights into the mechanisms involved in the desorption process near the growth interface. For weakly-binding atoms, it is found that the desorption behaviors are sensitive to the growth temperature. High temperature enhances desorption and reduces the sticking coefficient. More interestingly, when the temperature is high, the desorption behaviors of weakly binding atoms can be evidently affected by stoichiometry due to the dependence of surface binding on stoichiometry, while at low temperatures, the stoichiometry-dependent desorption vanishes. As the binding strength increases, the desorption behavior becomes less sensitive to the temperature and surface conditions and finally appears to be independent of temperature and stoichiometry. In addition, during film growth, new adsorbates can gradually modify the stoichiometry on the growth interface and consequently the surface binding, which may affect desorption behaviors as well. Therefore, the desorption behaviors are highly nonlinear with time, especially when γ_A/γ_B is small. Finally, it is also to be noted that the MD analyses in this work are by no means complete. Some issues, such as how the incident energy[57] and element segregation[58] affect the stoichiometry dependent desorption, are still unclear, and the effective ways to circumvent this disturbance in controlling the composition for vapor codeposition is also worthy of further investigations.

ACKNOWLEDGMENTS

This work is supported by the National Natural Science Foundation of China (NNSFC) (Grant No. 11302227) as well as by the Youth Innovation Promotion Association Chinese Academy of Science (CAS) (Grant No. 2015014). Funding from the Strategic Priority Research Program of the Chinese Academy of Sciences is also acknowledged. The computations were performed in the Computing Facility for Computational Mechanics, Institute of Mechanics, Chinese Academy of Sciences.

[1] S. Zhang, *Nanostructured Thin Films and Coatings: Functional Properties* (CRC Press, New York, 2010).
[2] C. Cepek, R. Macovez, M. Sancrotti, L. Petaccia, R. Larciprete, S. Lizzit, and A. Goldoni, Appl. Phys. Lett. **85**, 976 (2004).
[3] Z.-J. Wang, C. Liu, Z. Li, and T.-Y. Zhang, J. Appl. Phys. **108**, 083506 (2010).
[4] C. Huang, X. Peng, T. Fu, Y. Zhao, C. Feng, Z. Lin, and Q. Li, Appl. Surf. Sci. **392**, 215 (2017).
[5] H. Kindlund, D. G. Sangiovanni, J. Lu, J. Jensen, V. Chirita, I. Petrov, J. E. Greene, and L. Hultman, J. Vac. Sci. Technol. A **32**, 5 (2014).
[6] H. Kindlund, D. G. Sangiovanni, J. Lu, J. Jensen, V. Chirita, J. Birch, I. Petrov, J. E. Greene, and L. Hultman, Acta Mater. **77**, 394 (2014).
[7] H. Byrd, E. P. Suponeva, A. B. Bocarsly, and M. E. Thompson, Nature **380**, 610 (1996).
[8] F. B. Abdelrazzaq, R. C. Kwong, and M. E. Thompson, J. Am. Chem. Soc. **124**, 4796 (2002).
[9] A. Gozar, G. Logvenov, L. F. Kourkoutis, A. T. Bollinger, L. A. Giannuzzi, D. A. Muller, and I. Bozovic, Nature **455**, 782 (2008).
[10] M. Weisheit, S. Faehler, A. Marty, Y. Souche, C. Poinsignon, and D. Givord, Science **315**, 349 (2007).
[11] C. Liu, J. Zhang, L. Wang, Y. Shu, and J. Fan, Solid State Ion. **232**, 123 (2013).
[12] J. Fang, X. Z. Bi, D. J. Si, Z. Q. Jiang, and W. X. Huang, Appl. Surf. Sci. **253**, 8952 (2007).
[13] B. C. Zhu, P. F. Xia, Y. Li, W. K. Ho, and J. G. Yu, Appl. Surf. Sci. **391**, 175 (2017).

[14]Y. Dumont, N. Keller, E. Popova, D. S. Schmool, M. Tessier, S. Bhattacharya, B. Stahl, R. M. C. Da Silva, and M. Guyot, Phys. Rev. B **76**, 104413 (2007).
[15]K. Barmak, J. Kim, L. H. Lewis, K. R. Coffey, M. F. Toney, A. J. Kellock, and J. U. Thiele, J. Appl. Phys. **98**, 033904 (2005).
[16]R. Jaafar, D. Berling, D. Sebilleau, and G. Garreau, Phys. Rev. B **81**, 155423 (2010).
[17]M. R. Beebe, D. B. Beringer, M. C. Burton, K. Yang, and R. A. Lukaszew, J. Vac. Sci. Technol. A **34**, 021510 (2016).
[18]A. Kawano, H. Ishiwata, S. Iriyama, R. Okada, T. Yamaguchi, Y. Takano, and H. Kawarada, Phys. Rev. B **82**, 085318 (2010).
[19]C. S. Lue, Y. S. Tseng, J. Y. Huang, H. L. Hsieh, H. Y. Liao, and Y. K. Kuo, AIP Adv. **3**, 072132 (2013).
[20]H. Gueddaoui, S. Maabed, G. Schmerber, M. Guemmaz, and J. C. Parlebas, Eur. Phys. J. B **60**, 305 (2007).
[21]J. Shao, L. Tang, C. Edmunds, G. Gardner, O. Malis, and M. Manfra, J. Appl. Phys. **114**, 023508 (2013).
[22]J. Fan, I. D. Boyd, and C. Shelton, J. Vac. Sci. Technol. A **18**, 2937 (2000).
[23]D. M. Packwood, S. Shiraki, and T. Hitosugi, Phys. Rev. Lett. **111**, 036101 (2013).
[24]S. Morisset, F. Aguillon, M. Sizun, and V. Sidis, J. Chem. Phys. **121**, 6493 (2004).
[25]D. Edstrom, D. G. Sangiovanni, L. Hultman, I. Petrov, J. E. Greene, and V. Chirita, J. Vac. Sci. Technol. A **34**, 041509 (2016).
[26]D. G. Sangiovanni, P. Edstrom, L. Hultman, I. Petrov, J. E. Greene, and V. Chirita, Surf. Sci. **624**, 25 (2014).
[27]D. G. Sangiovanni, A. B. Mei, L. Hultman, V. Chirita, I. Petrov, and J. E. Greene, J. Phys. Chem. C **120**, 12503 (2016).
[28]J. A. Rodriguez, P. Liu, J. Dvorak, T. Jirsak, J. Gomes, Y. Takahashi, and K. Nakamura, J. Chem. Phys. **121**, 465 (2004).
[29]Y. Shirotori, K. Sawada, K. Ozawa, K. Edamoto, and S. Otani, Surf. Sci. **584**, 237 (2005).
[30]X. W. Sha, B. Jackson, and D. Lemoine, J. Chem. Phys. **116**, 7158 (2002).
[31]R. Martinazzo and G. F. Tantardini, J. Chem. Phys. **124**, 124702 (2006).
[32]M. Rose, J. W. Bartha, and I. Endler, Appl. Surf. Sci. **256**, 3778 (2010).
[33]R. Friedlein, A. Fleurence, J. T. Sadowski, and Y. Yamada-Takamura, Appl. Phys. Lett. **102**, 221603 (2013).
[34]Y. Han, B. Uenal, and J. W. Evans, Phys. Rev. Lett. **108**, 216102 (2012).
[35]F. Stokker-Cheregi, A. Nedelcea, M. Filipescu, A. Moldovan, D. Colceag, V. Ion, R. Birjega, and M. Dinescu, Appl. Surf. Sci. **257**, 5312 (2011).
[36]J. Zhu, P. Goetsch, N. Ruzycki, and C. T. Campbell, J. Am. Chem. Soc. **129**, 6432 (2007).
[37]T. Karabacak, H. Guclu, and M. Yuksel, Phys. Rev. B **79**, 195418 (2009).
[38]H. J. Kim, Y. Egashira, and H. Komiyama, Appl. Phys. Lett. **59**, 2521 (1991).
[39]N. Lopez, F. Illas, and G. Pacchioni, J. Am. Chem. Soc. **121**, 813 (1999).
[40]Y. D. Kim, T. Wei, S. Wendt, and D. W. Goodman, Langmuir **19**, 7929 (2003).
[41]C. Liu, L. H. Wang, Y. H. Shu, and J. Fan, in *Proceedings of the 29th International Symposium on Rarefied Gas Dynamics*, edited by J. Fan (American Institute of Physics, Melville, 2014), Vol. 1628, p. 439.
[42]See http://lammps.sandia.gov/index.html for molecular dynamics simulation code.
[43]Q. Li, X. Peng, T. Peng, Q. Tang, X. Zhang, and C. Huang, Appl. Surf. Sci. **357**, 1823 (2015).
[44]J. Zhang, C. Liu, Y. Shu, and J. Fan, Appl. Surf. Sci. **261**, 690 (2012).
[45]J. Zhang, C. Liu, and J. Fan, Appl. Surf. Sci. **276**, 417 (2013).
[46]B. C. Hubartt, X. Liu, and J. G. Amar, J. Appl. Phys. **114**, 083517 (2013).
[47]M. W. Finnis and J. E. Sinclair, Philos. Mag. A **50**, 45 (1984).
[48]C. Liu and Z. Li, Phys. Rev. Lett. **105**, 174501 (2010).
[49]C. Liu and Z. Li, Phys. Rev. E **80**, 036302 (2009).
[50]P. M. Agrawal, B. M. Rice, and D. L. Thompson, Surf. Sci. **515**, 21 (2002).
[51]D. G. Sangiovanni, Appl. Surf. Sci. **450**, 180 (2018).
[52]J. Li, J. W. Mayer, and E. G. Colgan, J. Appl. Phys. **70**, 2820 (1991).
[53]M. Gurvitch, L. Manchanda, and J. M. Gibson, Appl. Phys. Lett. **51**, 919 (1987).
[54]A. Beniya, K. Mukai, Y. Yamashita, and J. Yoshinobu, J. Chem. Phys. **129**, 016101 (2008).
[55]Y. Kitaguchi, S. Habuka, T. Mitsui, H. Okuyama, S. Hatta, and T. Aruga, J. Chem. Phys. **139**, 044708 (2013).
[56]L. W. Liu, K. Yang, W. D. Xiao, Y. H. Jiang, B. Q. Song, S. X. Du, and H. J. Gao, Appl. Phys. Lett. **103**, 023110 (2013).
[57]D. Edstrom, D. G. Sangiovanni, L. Hultman, I. Petrov, J. E. Greene, and V. Chirita, J. Appl. Phys. **121**, 025302 (2017).
[58]K. Song, Z. Li, H. Guo, Z. Xu, and S. Fan, J. Appl. Phys. **123**, 154107 (2018).

View publication stats